Computers and Electronics in Agriculture 179 (2020) 105837

Contents lists available at ScienceDirect

Computers and Electronics in Agriculture

journal homepage: www.elsevier.com/locate/compag

Development of an integrated 3R end-effector with a cartesian manipulator for pruning apple trees

Azlan Zahid [a,c], Md Sultan Mahmud [a,c], Long He [a,c,*], Daeun Choi [a], Paul Heinemann [a], James Schupp [b,c]

[a] Department of Agricultural and Biological Engineering, Pennsylvania State University, University Park, PA, United States
[b] Department of Plant Science, Pennsylvania State University, University Park, PA, United States
[c] Penn State Fruit Research and Extension Center (FREC), Biglerville, PA, United States

ARTICLE INFO

Keywords:
Apple (Malus x domestica Borkh.)
Manipulability
Pruning end-effector
Reachable workspace simulation
Robotic pruning

ABSTRACT

Robotic pruning is a potential solution to address the issues of labor shortages and high associated costs, but it has challenges due to the unstructured working environment. For successful robotic pruning, target branches have to be reached with fewer spatial requirements for the end-effector cutter and the manipulator. A three-rotational (3R) degrees of freedom (DoF) end-effector was designed considering maneuvering, spatial, mechanical, and horticultural requirements. Simulations were conducted with the end-effector to investigate the reachable workspace, the cutter frame orientation, and the manipulability index. The simulation results suggested that the proposed design has a spherical reachable workspace with a void due to the presence of a physical constraint of the linear arm. The manipulability index was determined to be independent of the rotation of the first and last joint of the end-effector. The prototype of the proposed end-effector was integrated with a cartesian manipulator. An Arduino-based control system was developed along utilizing a Matlab graphical user interface (GUI). A series of field tests were conducted on 'Fuji'/Bud. 9 apple trees with trellis-trained architecture. The field tests validated the simulation results, and the end-effector successfully cut branches up to ~25 mm diameter at wide range of orientations. This study provides the foundation for future investigations of branch accessibility for pruning with an integrated 3R end-effector and a cartesian manipulator system following a collision free trajectory.

1. Introduction

Apple is one of the biggest tree fruit commodities in the United States with the total economic impact of approximately $3.01 billion (USDA-NASS, 2019). Despite the huge economic impact, production operations for tree fruit such as thinning, harvesting, and pruning are still performed manually (Flood, 2006; Silwal, 2016). According to Marshall et al. (1993), pruning of a high density apple orchard required about 31 h of skilled labor per acre (0.4 ha). With increasing labor costs and limited labor availability, it is highly desirable to perform these production operations mechanically or robotically. Mechanical pruning (hedging) is a non-selective operation (Mika et al., 2016), so robotic pruning poses a potential solution for selective pruning of trees (Lehnert, 2012). However, the adoption of robotics to agriculture has enormous challenges. The currently available industrial robots can perform repetitive tasks with uniform objects in an unconstrained workspace, but agriculture is a constrained dynamic environment and the work objects vary in shape, size, position, and orientation (Simonton, 1991). Successful adoption requires integration between the robot's abilities and its working environment (Kondo & Ting, 1998; Simonton, 1991).

Studies have been reported on the adoption of robotics to improve sustainability of the fruit production (Hohimer et al., 2019; Li et al., 2020; Silwal et al., 2016; Tang et al., 2020). For robotic pruning, a vision system is essential for 3D reconstruction of the tree canopy, identification of tree branches to make pruning decisions, calculating coordinates of pruning points, and determining collision free path planning of the manipulator to reach target points. Many studies have focused on the 3D reconstruction for various robotic applications (Chen et al., 2020; Li et al., 2020), including apple tree pruning (Akbar et al., 2016; Chattopadhyay et al., 2016; Karkee et al., 2014; Li et al., 2016; Lindner et al., 2007; Medeiros et al., 2017). While, only a few were on the development of pruning robots such as an integrated manipulator and a vision system for the pruning of grapevines (Kondo et al., 1993; Botterill et al., 2017; *Vision Robotics Corporation*, 2015). These studies focused on canopies

* Corresponding author.

https://doi.org/10.1016/j.compag.2020.105837
Received 14 August 2020; Received in revised form 12 October 2020; Accepted 13 October 2020

with uniform architectures (He & Schupp, 2018) and no substantial contribution has been made for development of an apple tree pruning manipulation system.

A mechanical system for pruning trees includes a manipulation mechanism defined by the numbers and types of joints (R: revolute or P: prismatic) for positioning at a target, and an end-effector tool to perform pruning cuts. Kondo & Ting (1998) stated that the design configuration of the manipulators should be selected considering the specific work environment to reduce the risk of poor performance. Agricultural robots also deal with the random obstacles in the environment, and the efficiency to perform specific tasks is affected by the pose flexibility of the manipulator (Guo et al., 2015; Lin et al., 2017; Zahid et al., 2020b). Thus, the joint configuration should be selected carefully as it affects the pose flexibility of the manipulator for reaching a point in the workspace.

The end-effector is an integral unit of a robot to perform a specified task. The design characteristics and mechanism of the end-effector should be selected based on intended work (Kondo & Ting, 1998) as it greatly influences the efficiency of the robot (Bac et al., 2014). Some end-effectors have been developed in recent years to execute various tasks mainly for fruit harvesting (Jia et al., 2009; Kondo et al., 2010; Wang et al., 2016; Zhong et al., 2015) and thinning (Lyons et al., 2015). Robotic pruning of apple trees is challenging due to the crowded obstacle environment. The random orientation of the branches makes it difficult for the cutter to reach the target at a desirable orientation. Only a few studies have been reported for pruning end-effectors (Botterill et al., 2017; Huang et al., 2016; Zahid et al., 2020a). A 6 DoF robot with a mill-end cutter end-effector was developed for pruning vines (Botterill et al., 2017), but the mill-end cutter sometimes pushed the canes aside rather than cutting, and was unable to produce a separation cut. Zahid et al. (2020a) developed a compact end-effector using a pneumatic cylinder for pruning apple trees. The end-effector produced satisfactory results, but it only had 2R DoF with a three directional cartesian system, which limited its ability to reach all orientations. The key design considerations for a pruning end-effector include maneuverability in the task space, kinematic dexterity, and spatial, horticultural, and mechanical requirements (Huang et al., 2016; Zahid et al., 2020a). The time required by the end-effector to complete the specific task should be minimized to improve the efficiency of the robotic system (Wang et al., 2019). Furthermore, the smoothness of the pruning cut is essential as the rough-cut may cause branches to decay or otherwise negatively affect the healing process.

Based on the above-mentioned criteria, this study aimed to develop and evaluate the performance of a pruning end-effector. A three rotational (3R) shear cutter type pruning end-effector was designed in a 3D CAD environment considering the maneuverability, spatial, mechanical, and horticultural requirements for pruning apple trees. The kinematic model was established to simulate the reachable workspace, the end-effector cutter orientation, and the manipulability index of the end-effector. The end-effector was developed and integrated with a cartesian manipulator system. An Arduino-based control system was integrated with a Matlab interface to test the system in field conditions.

2. Material and methods

2.1. Robotic pruning system development

To attain all positions, the robot's DoF should be at least equal or greater than the task space dimensions. In the real world, the task space dimensions could not be greater than six, thus a 3R DoF pruning end-effector with a 3P DoF cartesian manipulator was developed to position the end effector cutter along the pruning branches.

2.1.1. 3R End-effector design

Designing an integrated end-effector for pruning trees is a critical task due to the dense working environment within the canopy. Although the pruning cut angle does not influence the re-growth of the branches (Schupp et al., 2019), the end-effector still has to reach the target position within a specific range of orientations to ensure placement of the branches in the shear cutter opening. The primary design criteria of the end-effector include maneuverability and spatial requirements to precisely position the cutter at a specific orientation with minimal space utilization. A pruning end-effector was designed by considering the 3R DoF (pitch, roll, and yaw) configuration to attain wide ranges of orientation (Fig. 1). The 3D CAD software SolidWorks (v.2020, Dassault Systèmes, Vélizy-Villacoublay, France) was used as a design tool to determine the most appropriate placement of components to minimize the dimensions of the end-effector. The model consists of three motors having the rotational axes perpendicular to each other. The rotational axis of joints θ_1, θ_2, and θ_3 was along the z, y, and x axis in global coordinates, respectively. A shear cutter was integrated with the end-effector as a cutting tool to produce a smooth and split-free pruning cut. Considering the diameter of apple tree branches (in most cases $<$25 mm), a shear cutter with a 60 mm front opening was used so that the branch was able to enter the cutter opening. The shear cutter tool was attached directly to the last joint(θ_3). The rotation of θ_1 and θ_2 changed the position and orientation, and the rotation of θ_3 only changed the orientation of the cutter. SolidWorks motion analysis was performed to examine the rotations, and to detect any interference or physical constraints in the designed end-effector. The maximum rotation limits for θ_1, θ_2, and θ_3 combining both clockwise and counterclockwise directions were 240°, 360°, and 360°, respectively. The mountings and frames for the integration of motors and the shear cutter were also designed using the SolidWorks motion analysis.

2.1.2. Integrated pruning system

The spatial requirement and the pose flexibility of the manipulator is very crucial for path planning to reach pruning points. During manipulation, the change in the pose greatly affects the spatial requirement of the system. Each joint and link of the manipulator contributes to a certain pose for reaching any target position and orientation. However, major variation in pose was observed for the positioning links of the manipulator, which affects the spatial requirement during maneuvering. Thus, to position the 3R end-effector in the proximity of target branches, a three DoF cartesian system was designed because of its minimum pose change attributes during manipulation. The integrated pruning system including the end-effector and the cartesian manipulator system is shown in Fig. 2. The order of joint placement was defined as prismatic joint L1: moves along the x-axis, prismatic joint L2: moves along the y-axis, and prismatic joint L3: moves along the z-axis in the global coordinates. In a previous study (Zahid et al., 2020a), the manipulator

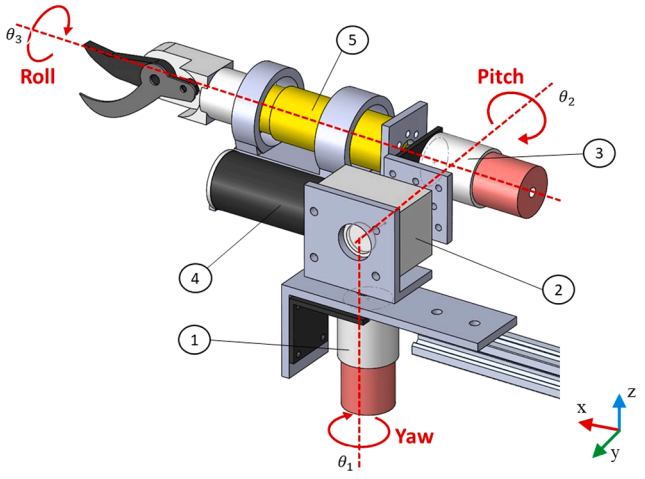

Fig. 1. Concept design of the end-effectors (components: 1. Motor for yaw (θ_1) rotation; 2. Motor for pitch (θ_2) rotation; 3. Motor for roll (θ_3) rotation; 4. Self-locking worm gearbox; 5. Shear cutter).

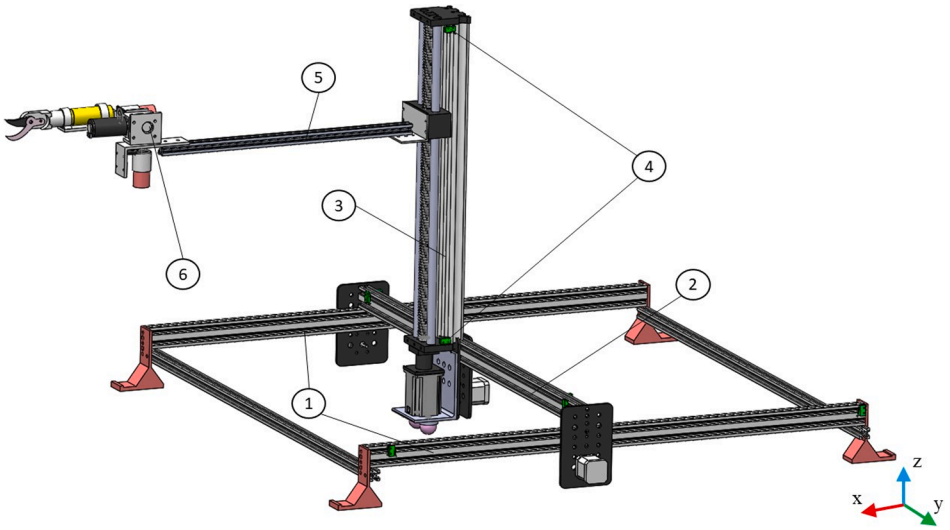

Fig. 2. Integrated pruning system with an end-effector attached to a cartesian manipulator; the components include: 1) x-axis rails; 2) y-axis rail; 3) z-axis linear actuator; 4) axis limit switches; 5) linear arm; 6) pruning end-effector.

system used three linear actuators without a rigid base platform, which resulted in vibration of the end-effector during operation. Therefore, a square base platform setup was selected to dampen the vibration and improve the stability of the of the system. The two sides of the square platform have a linear rail system for motion along the x-axis. A central linear rail for motion in the y-axis was attached end-to-end between the two linear rails of the x-axis. For motion along the z-axis, a linear actuator was attached to the linear rail of the y-axis. The motion in all three directions were independent of each other. A linear rigid arm was attached to the z-axis so that the cartesian manipulator could be placed outside the tree canopy, avoiding the interaction of the manipulator with the tree branches. The pruning end-effector was attached to the other end of the linear arm.

Prior to building a prototype, the motion animation tool in Solid-Works was used to detect any interference or physical constraints in the integrated manipulator system. The technical specifications of the components used to build the system are presented in Table 1. For the 3R end-effector, three DC motors were used. The mountings and frames for the motors and shear cutter were 3D printed in the laboratory. A flange coupling was used to connect the motor shafts and mountings. For the linear/cartesian system, the motion in the x and y axis was achieved by NEMA 17 stepper motors with a belt and pulley mechanism attached to the motor shaft. A NEMA 34 motor driven linear actuator was used for the z-axis motion. The larger motor was selected for the z-axis due to higher torque requirement to lift the linear arm and the integrated end-effector.

Table 1
Specifications of the components used for developing a prototype.

Item	Model/Type	Quantity	Specifications
End-effector motors for yaw pitch and roll θ_1, θ_2, and θ_3	For yaw and roll (θ_1 and θ_3) rotation: DC geared motors	3	For yaw and roll (θ_1 and θ_3) rotation: 12 V DC No-Load Speed 76 rpm, Rated torque 15Kg·cm
	For pitch (θ_2) rotation: DC geared motors with self-locking worm gearbox		For pitch (θ_2) rotation: 24 V DC, 74 rpm, Torque 25Kg·cm, worm gearbox: Gear ratio108:1
Cartesian motion	Slider/rails	4	Travel length x axis = 700 mm, y axis = 700 mm, z axis = 600 mm, 1.8 NEMA 17 24 V DC, 3A (NEMA 34 for z-axis)
Stepper/DC Driver	Bipolar/L298N	4 + 3	1.0–4.2A DC 20–50 V, Micro step (Steps/rev.) 400–25,600/H-bridge driver (dual) 0–36 mA, 5–35 V, 25 W
Shear cutter		1	12 V DC motor with hall sensor
Relay	Sun founder	1	4-Channel relay module, normally open
Limited switches	SN04-N	6	10–30 V DC, NPN

2.1.3. *Manipulation control for pruning*

A control system comprised of a microcontroller (Arduino Mega 2560, Arduino Inc.) and a user interface was developed to control the integrated pruning system. Fig. 3 illustrates the details of the control system. For the end-effector, the speed and direction of rotation of the motors were controlled by DC motor drivers, and those of the cartesian manipulator were controlled by stepper drivers. The limit switches were attached at the minimum and maximum limits of each axis of the cartesian manipulator system. A Graphical User Interface (GUI) was developed in Matlab (2019b, MathWorks, Mass., USA) and serial communication was established between the Matlab GUI and the Arduino microcontroller. The shear cutter in normal pose was set as 'open' to permit the branch to enter the cutter opening. A relay module was used to control the operation of the cutter. The connecting time for the relay was set to 0.75 s to complete the cut after the branch is placed within the cutter opening.

Fig. 4 represents the flowchart of the manipulation control process. The manipulator reached the target points using the forward kinematics of the system. The GUI requires manual inputs from the user to reach the target and operation of the cutter as the system was not equipped with a vision system to get the coordinates automatically. The control process for operating the system involved three basic function steps. The first step was to position the end-effector tool with the cartesian manipulator mechanism. The second step involved the rotation of the end-effector joints to reach the target pruning points with proper orientation of the cutter. The rotation of all motors occurs simultaneously. Once the cutter is properly aligned with the branch in its opening, the third step was to operate the shear by sending a signal to the relay module through the GUI. The same process was repeated for the next branch.

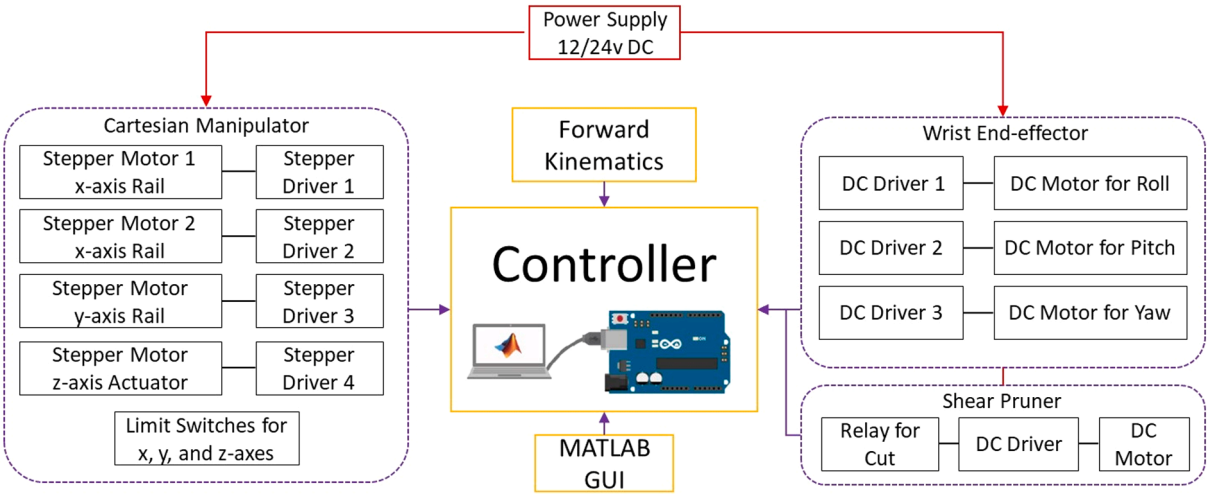

Fig. 3. Illustration of the integrated control system for the pruning end-effector and manipulator.

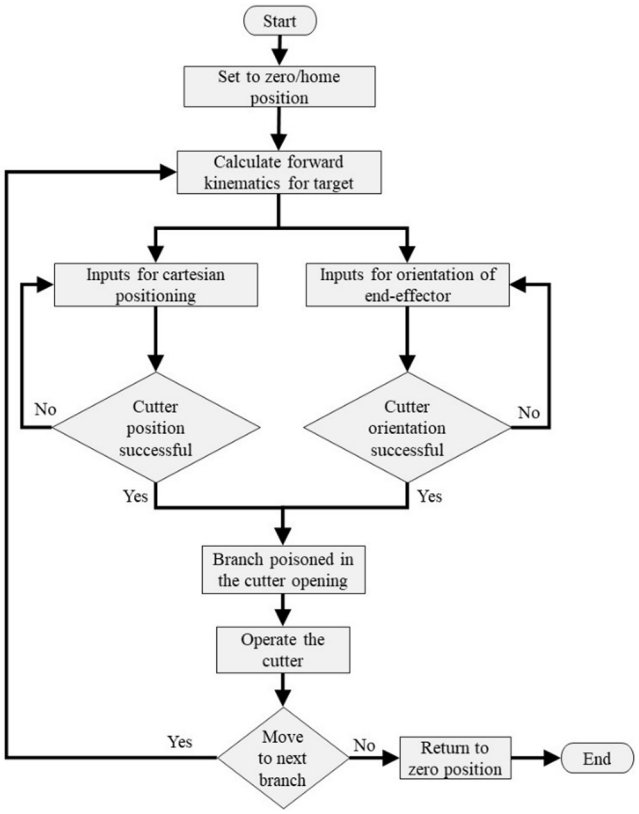

Fig. 4. Flowchart of the manipulation control process to reach pruning branches.

2.2. End-effector simulation

2.2.1. Kinematic model

The manipulator is defined by its degrees of freedom, type of joints, link length, link offset and link twist. The kinematic model of the manipulator was developed by calculating the Denavit-Hartenberg (DH) parameters (Table 2). Fig. 5 represents the coordinate frames of the integrated manipulator and end-effector. The first frame was defined as global coordinates frame O_G (x_g, y_g, z_g). The frames O_0 to O_2 were defined for the prismatic joints, the frames O_3 to O_5 represented the rotational joints, and the frame O_6 was defined at the center of the shear cutter; where the face of the cutter opening was aligned in the Z_6X_6

Table 2
DH parameters of the integrated pruning system.

Link	DH parameters				
	Joint angle θ_i (deg)	Link offset d_i (mm)	Link length a_i (mm)	Link twist α_i (deg)	Joint limit (mm/deg)
Link 1 (Manipulator base)	−90	$d_1 + L_1$	0	90	700
Link 2	90	$d_2 + L_2$	0	90	700
Link 3	0	$d_3 + L_3$	d4	0	600
Link 4 (End-effector base)	θ_1	d_5	0	90	240°
Link 5	$\theta_2 + 90$	d_6	0	90	360°
Link 6 (Cutter)	θ_3	d_7	0	0	360°

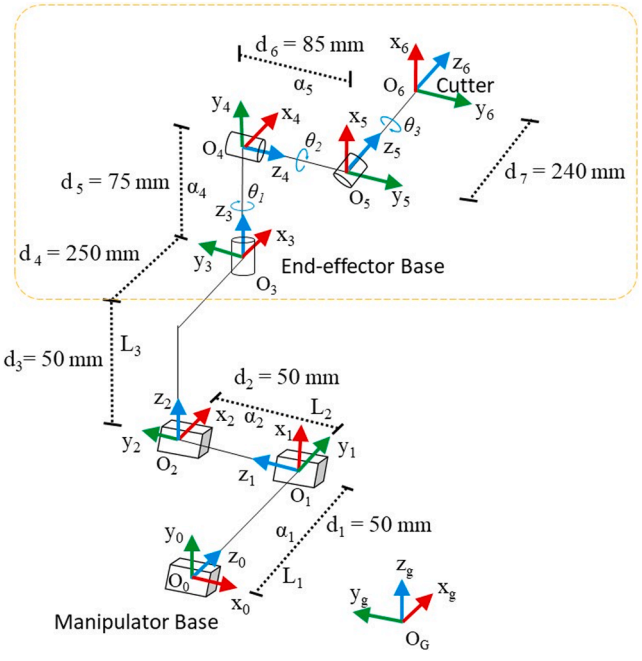

Fig. 5. Coordinate frames description of the integrated pruning system.

plane.

The coordinates of the end-effector cutter were calculated using homogenous transformation matrix equations (LaValle, 2006) considering the transformations between frame O_0 to O_6. The rotation along the z and x-axis were added to convert the end-effector cutter position to global coordinates. The position vector of the cutter frame (O_6) for the integrated end-effector (Link 4 to Link 6) in the global coordinates system was calculated as

$$P_{G,x} = d_7 \cdot \cos(\theta_2+90) \cdot \sin(\theta_1) + \sin(\theta_2+90) \cdot \cos(\theta_1) \quad (1)$$

$$P_{G,y} = -d_7 \cdot \cos(\theta_2+90) \cdot \cos(\theta_1) - \sin(\theta_2+90) \cdot \sin(\theta_1) \quad (2)$$

$$P_{G,z} = d_5 + d_7(-\cos(\theta_2+90)) \quad (3)$$

where, $P_{G,x}$ $P_{G,y}$ and $P_{G,z}$ are the coordinate values of the cutter in in the global x ,y, and z-coordinates respectively.

2.2.2. Simulation procedure

The kinematic model of the system was used to perform simulations for calculating and visualizing the reachable workspace, cutter frame orientations, manipulability index, and ellipsoids of the end-effector. The simulations were performed in the Matlab. The flowchart for the simulation algorithm is shown in Fig. 6. In the kinematic model, the joint limits for θ_1, θ_2, and θ_3 were added as 240°, 360°, and 360°, respectively. For all simulations, as the continuous iterations generate infinite numbers of datasets, a joint interval discretization function based on Monte-Carlo random sampling method (Abdolmalaki, 2017) was added to limit the number of dataset points. The workspace of a 3R end-effector is defined as radial and axial reach of the tool tip with respect to the reference frame (Ceccarelli, 1996). Thus, the joint variables θ_1, θ_2, and θ_3 were iterated in loops to plot the tool tip positions. Another function was created to track and plot the cutter frame orientations at all reachable workspace points using the rotation part of the transformation matrix. Manipulability (Yoshikawa, 1985) is a widely accepted kinematic performance measure index of the manipulator (Patel and Sobh, 2015). To analyze the ill-conditioning of the end-effector, the manipulability index simulation was performed using the function '*maniplty*()' in Matlab's Robotics and Vision Toolbox. The joint variables θ_1, θ_2, and θ_3 were iterated in a loop to calculate and plot the manipulability at different joint angles. Similarly, the velocity ellipsoid (closely related to the manipulability index) was a measure to determine the performance of manipulator, which provided the direction of feasible motion. The toolbox function '*vellipse*()' was used to generate and plot the velocity ellipsoid for the end-effector.

2.3. Experiment of the integrated pruning system

The integrated system was designed for pruning in high density apple orchards. The primary branches are usually widely spaced apart, and relatively smaller compared to conventional trees (<25 mm in most

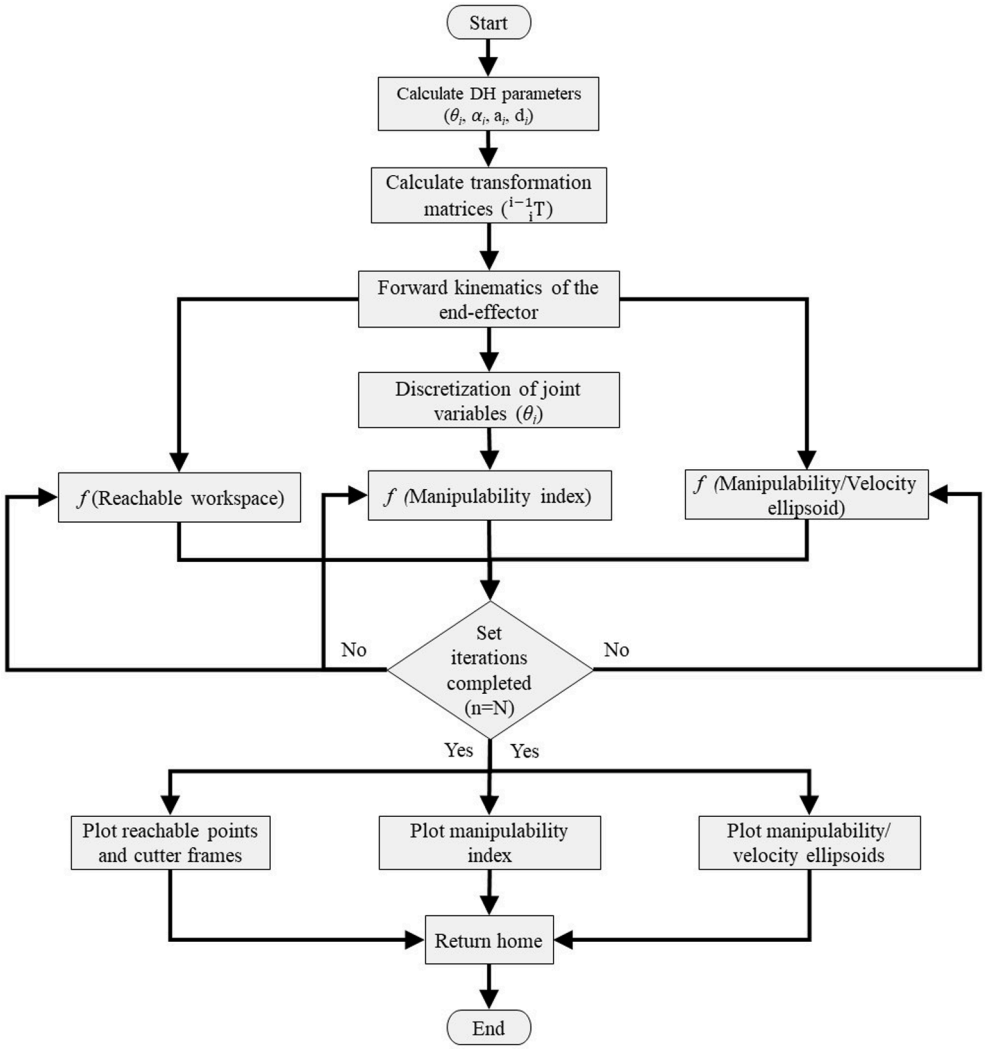

Fig. 6. Flowchart for the simulation process of the pruning end-effector.

cases). This high-density planting and narrow tree canopy architecture embrace the adoption of the robotic pruning system. The aim of the manipulator development was to cut the branches according to the pruning rules based on the limb to trunk ratio, which sets the criteria for the removal of branches greater than a specified diameter. This approach addresses up to 70% of the pruning load (Schupp et al., 2017). To evaluate system performance, field tests were conducted on trellised 'Fuji'/Bud. 9 apple trees trained to a fruiting wall architecture at Penn State's Fruit Research and Extension Center (FREC, Biglerville, Pennsylvania). The experimental setup of the system is shown in Fig. 7. The field tests were conducted to validate the simulation results of maneuvering and cutter orientations. During the field tests, about 100 cuts were applied on branches at a wide array of orientation ranges. A set of ten apple trees were selected randomly from the same orchard block. For each tree, about ten branches of different positions and orientations were selected. The coordinates of the cut points and the orientation of branches were estimated manually from the fixed manipulator base and entered through the GUI. Some cuts were applied approximately 10 to 20 mm from the tree trunk to evaluate the end-effector cutter capability to prune the branches close to the trunk. The branch diameter at the cut point and joint variables (θ_1, θ_2, and θ_3) were recorded to validate the design parameters of the integrated pruning system including maneuvering ability and spatial and horticultural requirements.

3. Results and discussion

3.1. Simulation results for the end-effector

3.1.1. Reachable workspace simulation

The simulation results for the end-effector reachable workspace shown in Fig. 8 presents the position coordinates of the end-effector tool tip in the task space. The robot links or revolute joints of the end-effector were in the home position as defined in the DH parameters.

The reachable workspace points of the end-effector are shown in Fig. 8(a). As the rotational axis of the end-effector joints were aligned perpendicular to each other, with the simultaneous rotation of θ_1, θ_2, and θ_3, the end-effector tool tip generated a spherical workspace envelop with a diameter of 240 mm, which is equal to the length of the last link (d_7). However, the simulation shows a void in the workspace envelope due to the rotational limit of the joint θ_1, which was set to 240° to avoid physical collision of the end-effector with the linear arm. Fig. 8 (b) shows the cutter frame orientations at reachable points in the workspace. As mentioned before, the end-effector cutter was aligned along Z_6X_6 plane (Fig. 5) where the z-axis is shown in blue and the x-axis is shown in red. In this simulation, random sampling was used to discretize and limit the number of datasets points, reducing the number of cutter frames against each point. The simulation shows that the cutter frame can attain multiple orientations at each point on the workspace envelope. Similarly, Fig. 8(c) shows the simulation results including the third axis (y-axis) of the cutter frame. The figure represents the possible orientations that the y-axis of the cutter frame can attain at each point (green line). To perform the pruning operation, the cutter plane (Z_6X_6) aligns with the branch at an angle, ideally perpendicular, which makes the branch parallel to the y-axis of the cutter frame. The figure shows that the cutter can be rotated a complete 360° around its axis at each reachable point on the workspace envelope, which demonstrates the ability to position for branches of various orientation ranges in the cutter opening.

3.1.2. Manipulability simulation

The manipulability and velocity ellipsoid are the kinematic performance indices to determine the performance of the manipulator at different sets of joint angles. The manipulability index ranges from 0 to 1, where 1 refers to the maximum manipulability and 0 refers to the minimum manipulability (singularity).

Fig. 9(a) shows the results of manipulability index of the end-effector with the three revolute joints (θ_1, θ_2, and θ_3) rotated separately from lower to upper limits. The manipulability of the end-effector was independent of the first and last joint (θ_1 and θ_3). When the middle joint (θ_2) was at the zero or ±180° position, the manipulability index was '1'. At this point, the end-effector can make full use of all DoFs. The manipulability index of the end-effector was reduced equally when the rotation of θ_2 was applied in either direction (CW or CCW). The lowest index of '0′ was observed when θ_2 reaches ±90°. Fig. 9(b) shows the variation in the manipulability index with simultaneous rotation of two joint angles. Similar results were obtained showing that the manipulability index becomes '0' as θ_2 reached ±90°, referred to as end-effector singularity. At this position, the end-effector loses one of its DoF as the axis of rotation for θ_1 and θ_3 becomes parallel. The result is an infinite number of inverse kinematic solutions, leading to end-effector movement in an unexpected direction. Specifically, the end-effector cutter will be pointing in the global z-axis and the lost DoF will be the global x-axis. However, the situation of the cutter pointing upwards or downwards is very unlikely to occur as the pruning path can be planned on the horizontal plane to avoid singularity. Approach of the device to the singularity can be detected and a singular value decomposition (SVD) controller can be built to identify the degenerated dimensions, reducing the forces to 0 in the undesirable direction based on the values of the manipulability index.

The velocity ellipsoid is a similar measure to the manipulability index but it defines the directions of feasible motion for the end-effector in global coordinates. Fig. 10 shows simulation results of ellipsoids calculated using the rotation of only θ_2, in a set of three pairs as yz, xz, and xy of the global coordinates, respectively. The figure shows that the maximum diameter of the ellipsoid exists in the yz plane. It suggests that when θ_2 is at home position i.e. 0° or 180°, the end-effector will have

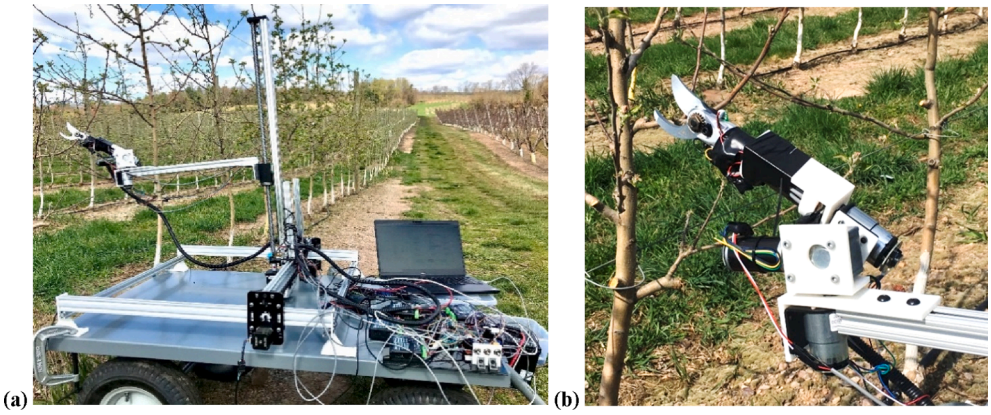

Fig. 7. Experimental setup in the apple orchard. (a) Integration pruning system, (b) Pruning end-effector.

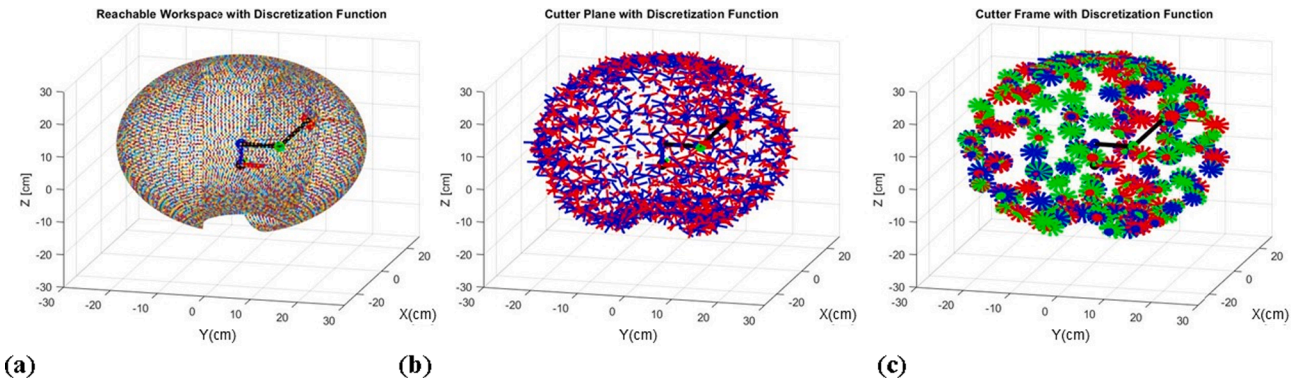

Fig. 8. Reachable workspace for the integrated end-effector with (a) Reachable points, (b) Cutter face planes, (c) Cutter tool frames.

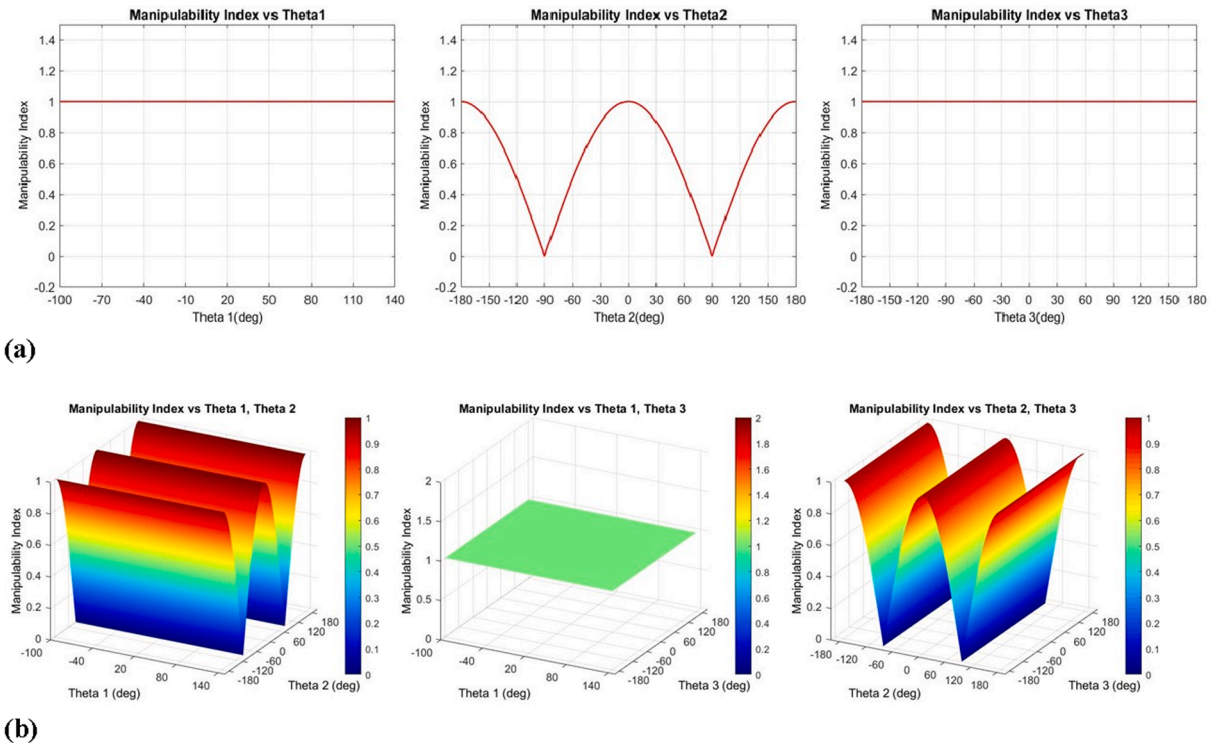

Fig. 9. Manipulability index of the integrated end-effector. (a) Each joint variable, (b) Combined variation in joint variables.

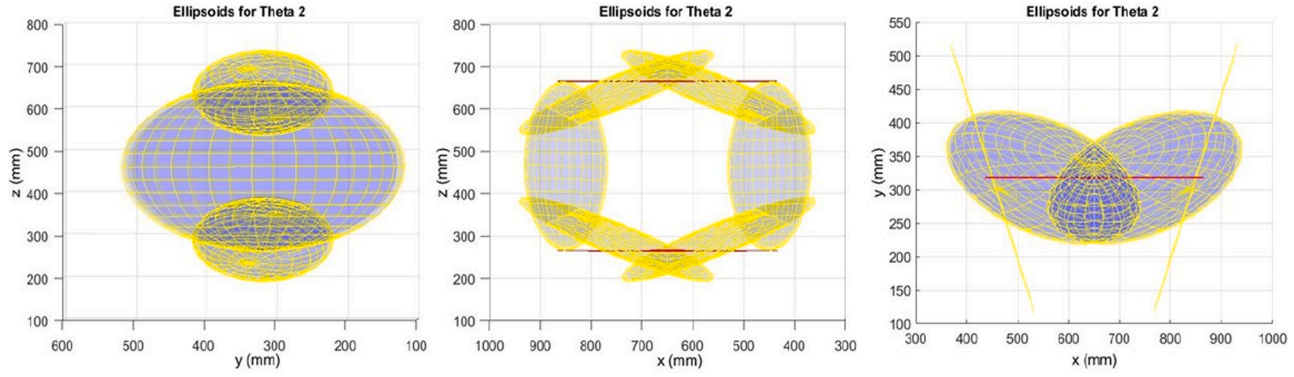

Fig. 10. Manipulability Ellipsoids with rotation of θ_2 at yz, xz, and xy coordinate planes.

maximum manipulability and velocity in the yz plane. The shear cutter in the home configuration points into the global yz plane (Fig. 5). When θ_2 rotates $\pm 90^{\circ}$, the shear cutter points directly upwards or downwards, and the ellipsoid will move to the xy plane. As the manipulability becomes zero (red line), the ellipsoid can no longer be generated, which suggests that the end-effector cannot move in one of the global axes. However, it is the very unlikely that the cutter will point upwards or downwards for pruning the branches. These simulation results are useful for efficient trajectory planning by considering the placement of a manipulator with respect to a target tree. For example, to gain maximum benefit of the highest manipulability/velocity region (yz plane), the target tree must be approached or placed in the direction of the global x-axis for the trajectory planning.

3.2. Results from field experiments

Field tests were conducted to validate the performance of the simulation results. Approximately 100 cuts were applied to branches at different positions and orientations. All joint positions (θ_1, θ_2, and θ_3) were recorded for reaching each pruning location for validation of reachable workspace and cutter orientation. Table 3 lists the angular positions of the joints for cutting these targeted branches when the cutter plane was approximately perpendicular to the branches. During the test, it was observed that the end-effector successfully reached all selected branches with a proper cutter orientation. Another design parameter was the time required to perform the actual cutting operation once the branch is positioned in the cutter opening. With the relay time set as 0.75 s, the cutter was able to fully cut all the branches. The diameter of the pruned branches at the point of cut is also presented in the table. The system achieved smooth and split-free cuts for branches up to 25 mm diameter. The results showed that the system reached all the test branches with the three joint angles adjusted. The maximum rotation angles for all joints were also recorded during the experiment to validate the workspace simulation. The joint variable (θ_1) followed the limits added in the Matlab GUI to prevent collision with the linear arm. At the upper and lower limits of θ_1, the end-effector cutter tip was approximately 50 mm in proximity of the physical constraint (linear arm). No self-collision or physical interference was observed with rotation of θ_2 and θ_3. Due to the joint limit for θ_1, a void in the reachable workspace was observed. However, the system was able to reach all the target cut points. The target points were reached with manual entries, while even with the automatic trajectory, the void will not negatively affect the performance of the system as it appears on the negative x-axis of global coordinates (position of the linear arm). It is very unlikely to prune the branches by rotating the cutter facing backwards. Even with this situation, the cartesian system can move the end-effector backwards along the negative x-axis, which will result in positioning the target branches in the front side of the cutter. Overall, the integrated pruning system complied with the design criteria to position the cutter properly with branches of wide orientations. Tests also revealed that with the rotation of the last joint (θ_3) at any point on the workspace, the cutter was aligned perpendicular or with a certain angle with the branches.

Table 3
Data subset from the field experiment of the end-effector performance assessment.

Test	Branch diameter (mm)	Angle θ_1 (deg)	Angle θ_2 (deg)	Angle θ_3 (deg)	[a]Cut point coordinates (x, y, z)
1	12	30	40	25	(480, 525, 390)
2	17	65	75	−10	(615, 475, 410)
3	09	45	55	15	(420, 645, 535)
4	13	−20[d]	−25	15	(340, 325, 265)
5	16	−35	70	00[c]	(388, 415, 492)
6	17	15	40	−45	(362, 690, 425)
7	15	75	45	−20	(380, 546, 365)
8	21	40	65	00	(315, 590, 405)
9	12	65	75	15	(315, 435, 545)
10	08	35	−20	−45	(605, 240, 380)
11	16	45	45	90	(450, 530, 435)
12	25[b]	40	−25	15	(635, 390, 325)
13	19	65	35	−45	(380, 485, 368)
14	22	15	00[b]	75	(550, 371, 325)
15	14	55	55	30	(475, 595, 360)
16	18	30	40	90	(595, 625, 410)
17	11	−15	25	45	(710, 525, 375)
18	19	00[b]	55	00	(545, 615, 365)
19	23	−25	15	75	(565, 440, 475)
20	16	55	30	45	(615, 645, 415)

[a] Estimated coordinates calculated manually.
[b] Maximum branch diameter recorded.
[c] θ_1, θ_2, and θ_3 at '0' is referred as home position.
[d] Negative sign indicates CW movement.

During the test, the cuts were applied at random locations on selected branches, some in the middle, and some at the base or close to the tree trunk. It was observed that when the target point was close to the trunk and only the perpendicular cutting posture was considered, the cutter could collide with the trunk. In this case, the cutter pose was rotated to find a suitable orientation to cut the branch at the same point. During the test, majority of the branches were cut with perpendicular cutter posture, while some were cut with an adjusted angle, providing bevel cuts which would not affect the regrowth (Schupp et al., 2019). However, when the cutter plane and branch axis were not perpendicular or the cutter was tilted with respect to branches, the effective cutter opening for the branches to enter was greatly reduced, which increased the chance of missing the target branch. Thus, for automatic trajectory planning, the perpendicular cutter approach should be selected as an ideal case to utilize the maximum opening width of the cutter. Other alternate poses can be selected if the ideal approach is not feasible due to the complex workspace environment or when the target is near a trunk. Apple trees have a complex canopy structure with branches at random orientations, leading to the challenge of maneuvering the end-effector in the task space. From the workspace simulation and field tests, it was observed that the end-effector attained a wide range of orientations while utilizing a small workspace during maneuvering within the canopy. Once the cutter was in proximity of the target point, the effective change in spatial requirements of the system only depended on the last link length.

The orientation of the branch should be known for the alignment of the cutter at target cut points, but the system was not integrated with a vision system. Typically, multiple attempts were required to correctly position the branches within the cutter opening, which could lead to low efficiency due to increased cycle time for each pruning cut. The shear cutter was able to produce a split-free smooth cut up to 25 mm diameter without pushing the branches. For pruning in modern high-density orchards with frequent branch renewal, the diameter of the pruning branches usually falls in the successful cutting diameter range of the developed end effector (Schupp et al., 2017). However, an accurate sensing information is essential to make the pruning decision using predefined pruning rules. In the future, a machine vision system will be integrated to accurately detect the pruning point coordinates as well as orientation of the branches to generate a collision-free path to reach target points. The accurate sensing of the environment is anticipated to reduce the cycle time, and the overall performance of the robotic pruning system could be improved.

The manipulability and velocity ellipsoid relates to the inverse kinematics and singularities of the system. At singularity, the manipulator loses one of its degrees of freedom, which limits its movement in one of the task space directions. The joint configuration and arrangement determine the singular region of the manipulator in the workspace; thus, the configuration should be selected to minimize the incidence of singularities. For example, in the proposed design, the singularity occurs when the cutter points straight up or down ($\theta_2 = \pm 90^{\circ}$), and it is very unlikely to cut the branches with the cutter pointing upwards or

downwards. Similarly, the manipulator trajectory should be planned in accordance with the simulation results of these indices for better performance of the system. At this stage, validation was not performed as the branch orientation information was required for trajectory planning, consequently the system was operated using forward kinematics through GUI. However, the results of manipulability and ellipsoid tests are vital for automatic path planning, which will be used in further studies.

Most of previous robotic pruning research focused on tree canopy reconstruction (Akbar et al., 2016; Chattopadhyay et al., 2016; Karkee et al., 2014; Medeiros et al., 2017), and only a few on the manipulation or collision-free path planning for robotic pruning (Botterill et al., 2017; Zahid et al., 2020a; Zahid et al., 2020b). The work presented in this paper provides guidelines for designing an end-effector integrated with a cartesian manipulator for robotic pruning. Although the collision of the end-effector with branches was also observed during the experiment, the integrated system performed well for the identified design criteria. Meanwhile, it required accurate information about the coordinates of cut points, and orientation of branches for automatic path planning and collision avoidance. The system needs to be integrated with a vision system for 3D reconstruction of branches. With good sensing of the environment and path planning using known branch coordinates and orientation, the efficiency of the system for positioning and aligning the cutter tool will be improved. Furthermore, an inertial measurement unit (IMU) should also be integrated to consider ground conditions for developing a robotic pruning system.

4. Conclusions

A 3R DoF end-effector was developed and integrated with a cartesian manipulator to perform pruning on high density apple orchards. A kinematic model was developed to perform the simulation for calculating the reachable workspace, achievable cutter orientations, manipulability, and velocity ellipsoids. The workspace simulation showed that the end-effector has a void in the reachable workspace due to the presence of a physical constraint (linear arm). The simulation for tracking the cutter frame orientation demonstrated the capability of the end-effector to attain multiple orientations at each point on the reachable workspace. Meanwhile, the designed end-effector exhibited good manipulability, and the results of manipulability or velocity ellipsoids could be used for avoiding singularities during automatic path planning. The field tests proved that the end-effector cutter can reach the branches at wide orientation ranges and the reachability of the end-effector was not affected by the workspace void as it was integrated with a cartesian manipulator. The shear cutter was able to produce a smooth cut for the branches up to 25 mm diameter, supporting the suitability of the end-effector for pruning high density apple trees. Future studies will be conducted for the collision-free path planning of the integrated manipulator end-effector system using different algorithms such as RRT, RRT connect, and Genetic Algorithm (GA). A vision system will also be developed for the 3D reconstruction of the tree canopy, and the pruning decision rules will be in-cooperated to accurately locate the pruning points, which is essential to develop an integrated robotic pruning system.

CRediT authorship contribution statement

Azlan Zahid: Conceptualization, Investigation, Methodology, Validation, Writing - original draft. **Md Sultan Mahmud:** Investigation, Methodology, Validation. **Long He:** Conceptualization, Supervision, Writing - review & editing, Funding acquisition. **Daeun Choi:** Supervision, Writing - review & editing. **Paul Heinemann:** Supervision, Writing - review & editing. **James Schupp:** Supervision, Writing - review & editing.

Declaration of Competing Interest

The authors declare that they have no known competing financial interests or personal relationships that could have appeared to influence the work reported in this paper.

Acknowledgments

This research was partially supported in part by United States Department of Agriculture (USDA)'s National Institute of Food and Agriculture Federal Appropriations under Project PEN04547 and Accession No. 1001036. We also would like to give our special thanks for the support from Penn State College of Agricultural Sciences Stoy G. and Della E. Sunday program and Northeast Sustainable Agriculture Research and Education (SARE) Graduate Student Grant GNE19-225-33243.

References

Abdolmalaki, R.Y., 2017. Development of direct kinematics and workspace pepresentation for Smokie robot manipulator & the barret WAM, pp. 1–7. http://arxiv.org/abs/1707.04820.

Akbar, S.A., Elfiky, N.M., Kak, A., 2016. A novel framework for modeling dormant apple trees using single depth image for robotic pruning application. In: 2016 IEEE International Conference on Robotics and Automation (ICRA), pp. 5136–5142. https://doi.org/10.1109/ICRA.2016.7487718.

Bac, C.W., Hemming, J., van Henten, E.J., 2014. Stem localization of sweet-pepper plants using the support wire as a visual cue. Comput. Electron. Agric. 105, 111–120. https://doi.org/10.1016/j.compag.2014.04.011.

Botterill, T., Paulin, S., Green, R., Williams, S., Lin, J., Saxton, V., Mills, S., Chen, X.Q., Corbett-Davies, S., 2017. A robot system for pruning grape vines. J. Field Rob. 34 (6), 1100–1122. https://doi.org/10.1002/rob.21680.

Ceccarelli, M., 1996. A formulation for the workspace boundary of general N-revolute manipulators. Mech. Mach. Theory 31 (5), 637–646.

Chattopadhyay, S., Akbar, S.A., Elfiky, N.M., Medeiros, H., Kak, A., 2016. Measuring and modeling apple trees using time-of-flight data for automation of dormant pruning applications. In: 2016 IEEE Winter Conference on Applications of Computer Vision (WACV), pp. 1–9. https://doi.org/10.1109/WACV.2016.7477596.

Chen, M., Tang, Y., Zou, X., Huang, K., Huang, Z., Zhou, H., Wang, C., Lian, G., 2020. Three-dimensional perception of orchard banana central stock enhanced by adaptive multi-vision technology. Comput. Electron. Agric. 174, 105508. https://doi.org/10.1016/j.compag.2020.105508.

Flood, S., 2006. Design of a robotic citrus harvesting end-effector and Force. University of Florida.

Guo, Y., Dong, H., Ke, Y., 2015. Stiffness-oriented posture optimization in robotic machining applications. Rob. Comput. Integr. Manuf. 35, 69–76. https://doi.org/10.1016/j.rcim.2015.02.006.

He, L., Schupp, J., 2018. Sensing and automation in pruning of apple trees: a review. Agronomy 8 (10), 211. https://doi.org/10.3390/agronomy8100211.

Hohimer, C.J., Wang, H., Bhusal, S., Miller, J., Mo, C., Karkee, M., 2019. Design and field evaluation of a robotic apple harvesting system with a 3D-printed soft-robotic end-effector. Trans. ASABE 62 (2), 405–414. https://doi.org/10.13031/trans.12986.

Huang, B., Shao, M., Chen, W., 2016. Design and research on end effector of a pruning robot. Int. J. Simulation – Syst. Sci. Technol. 17 (36), 1–5. https://doi.org/10.5013/IJSSST.a.17.36.19.

Jia, B., Zhu, A., Yang, S.X., Mittal, G.S., 2009. Integrated gripper and cutter in a mobile robotic system for harvesting greenhouse products. In: 2009 IEEE International Conference on Robotics and Biomimetics (ROBIO), pp. 1778–1783. https://doi.org/10.1109/ROBIO.2009.5420430.

Karkee, M., Adhikari, B., Amatya, S., Zhang, Q., 2014. Identification of pruning branches in tall spindle apple trees for automated pruning. Comput. Electron. Agric. 103, 127–135.

Kondo, N., Shibano, Y., Mohri, K., Monta, M., 1993. Basic studies on robot to work in vineyard 1: manipulator and harvesting hand. J. Jpn. Soc. Agric. Mach. 55, 85–94.

Kondo, N., Ting, K.C., 1998. Robotics for plant production. Artif. Intell. Rev. 12 (1–3), 227–243. https://doi.org/10.1007/978-94-011-5048-4_12.

Kondo, N., Yata, K., Iida, M., Shiigi, T., Monta, M., Kurita, M., Omori, H., 2010. Development of an End-effector for a tomato cluster harvesting robot. Eng. Agric. Environ. Food 3 (1), 20–24. https://doi.org/10.1016/S1881-8366(10)80007-2.

LaValle, S.M., 2006. Planning algorithms. In University of Illinois, first ed. Cambridge University Press. https://doi.org/10.1017/CBO9780511546877.

Lehnert, R., 2012. Robotic pruning. Good Fruit Grower Nov. 1, 2012. https://www.goodfruit.com/robotic-pruning/.

Li, F., Chattopadhyay, S., Akbar, S.A., Elfiky, N.M., Kak, A., 2016. A novel visualization tool for evaluating the accuracy of 3D sensing and reconstruction algorithms for automatic dormant pruning applications. In: 2016 IEEE Conference on Computer Vision and Pattern Recognition Workshops (CVPRW), pp. 338–346. https://doi.org/10.1109/CVPRW.2016.49.

Li, J., Tang, Y., Zou, X., Lin, G., Wang, H., 2020. Detection of fruit-bearing branches and localization of litchi clusters for vision-based harvesting robots. IEEE Access 8, 117746–117758. https://doi.org/10.1109/ACCESS.2020.3005386.

Lin, Y., Zhao, H., Ding, H., 2017. Posture optimization methodology of 6R industrial robots for machining using performance evaluation indexes. Rob. Comput. Integr. Manuf. 48, 59–72. https://doi.org/10.1016/j.rcim.2017.02.002.

Lindner, M., Kolb, A., Hartmann, K., 2007. Data-fusion of PMD-based distance-information and high-resolution RGB-images. In: 2007 International Symposium on Signals, Circuits and Systems, vol. 1, pp. 1–4. https://doi.org/10.1109/ISSCS.2007.4292666.

Lyons, D.J., Heinemann, P.H., Schupp, J.R., Baugher, T.A., Liu, J., 2015. Development of a selective automated blossom thinning system for peaches. Trans. ASABE 58 (6), 1447–1457. https://doi.org/10.13031/trans.58.11138.

Marshall, D., Maib, K., Peterson, B., Hinman, H., 1993. Estimated cost and returns of replanting an apple orchard to a double row v-trellis high density system in central Washington. http://ses.wsu.edu/wp-content/uploads/2018/10/EB1735.pdf.

Medeiros, H., Kim, D., Sun, J., Seshadri, H., Akbar, S.A., Elfiky, N.M., Park, J., 2017. Modeling dormant fruit trees for agricultural automation: modeling dormant fruit trees for agricultural automation. J. Field Rob. 34 (7), 1203–1224. https://doi.org/10.1002/rob.21679.

Mika, A., Buler, Z., Treder, W., 2016. Mechanical pruning of apple trees as an alternative to manual pruning. Acta Scientiarum Polonorum - Hortorum Cultus 15 (1), 113–121.

Patel, S., Sobh, T., 2015. Manipulator performance measures - a comprehensive literature survey. J. Intell. Robotic Syst.: Theory Appl. 77 (3-4), 547–570. https://doi.org/10.1007/s10846-014-0024-y.

Schupp, J.R., Winzeler, H.E., Kon, T.M., Marini, R.P., Baugher, T.A., Kime, L.F., Schupp, M.A., 2017. A method for quantifying whole-tree pruning severity in mature tall spindle apple plantings. HortScience Horts 52 (9), 1233–1240. https://doi.org/10.21273/HORTSCI12158-17.

Schupp, J.R., Winzeler, H.E., Schupp, M.A., 2019. Stub length and stub angle did not influence renewal shoot number or branch angle of tall spindle 'Gala'/Malling 9 apple trees. HortTechnology Hortte 29 (1), 46–49. https://doi.org/10.21273/HORTTECH04218-18.

Silwal, A., 2016. Machine vision system for robotic apple harvesting in fruiting wall orchards. Washington State University.

Silwal, A., Davidson, J., Karkee, M., Mo, C., Zhang, Q., Lewis, K., 2016. Effort towards robotic apple harvesting in Washington State. Paper Number: 162460869, St. Joseph, MI: ASABE. https://doi.org/10.13031/aim.20162460869.

Simonton, W., 1991. Robotic end effector for handling. 34(December), 2615–2621.

Tang, Y., Chen, M., Wang, C., Luo, L., Li, J., Lian, G., Zou, X., 2020. Recognition and localization methods for vision-based fruit picking robots: a review. Front. Plant Sci. 11 (May), 1–17. https://doi.org/10.3389/fpls.2020.00510.

USDA-NASS, 2019. Noncitrus Fruits and Nuts 2018 Summary, United States Department of Agriculture - National Agricultural Statistics Service. Washington, DC, USDA-NASS. Retrieved from https://www.nass.usda.gov/Publications/Todays_Reports/reports/ncit0619.pdf.

Wang, G., Yu, Y., Feng, Q., 2016. Design of end-effector for tomato robotic harvesting. IFAC-PapersOnLine 49 (16), 190–193. https://doi.org/10.1016/j.ifacol.2016.10.035.

Wang, Y., Yang, Y., Yang, C., Zhao, H., Chen, G., Zhang, Z., Fu, S., Zhang, M., Xu, H., 2019. End-effector with a bite mode for harvesting citrus fruit in random stalk orientation environment. Comput. Electronics Agric., 157, 454–470. https://doi.org/10.1016/j.compag.2019.01.015.

Yoshikawa, T., 1985. Manipulability of robotic mechanisms, pp. 439–446.

Zahid, A., He, L., Choi, D.D., Schupp, J., Heinemann, P., 2020. Collision free path planning of a robotic manipulator for pruning apple trees. ASABE Paper No. 200439. St. Joseph, MI: ASABE. https://doi.org/10.13031/aim.202000439.

Zahid, A., He, L., Zeng, L., Choi, D., Schupp, J., Heinemann, P., 2020b. Development of a robotic end-effector for apple tree pruning. Trans. ASABE 63 (4), 847–856. https://doi.org/10.13031/trans.13729.

Zhong, H., Nof, S.Y., Berman, S., 2015. Asynchronous cooperation requirement planning with reconfigurable end-effectors. Rob. Comput. Integr. Manuf. 34, 95–104. https://doi.org/10.1016/j.rcim.2014.11.004.